Nanomorphology of Bulk Heterojunction Photovoltaic Thin Films Probed with Resonant Soft X-ray Scattering

ARTICLE *in* NANO LETTERS · AUGUST 2010

Impact Factor: 13.59 · DOI: 10.1021/nl1009266 · Source: PubMed

NANO LETTERS

pubs.acs.org/NanoLett

Nanomorphology of Bulk Heterojunction Photovoltaic Thin Films Probed with Resonant Soft X-ray Scattering

Sufal Swaraj,[†,||] Cheng Wang,[‡] Hongping Yan,[†] Benjamin Watts,[†,#] Jan Lüning,[§,▽] Christopher R. McNeill,*[,||] and Harald Ade*[,†]

[†]Department of Physics, North Carolina State University, Raleigh, North Carolina 27695, [‡]Advanced Light Source, Lawrence Berkeley National Laboratory, Berkeley, California 94720, [§]Stanford Synchrotron Radiation Lightsource, Menlo Park, California 94025, and [||]Cavendish Laboratory, Department of Physics, University of Cambridge, J J Thomson Avenue, Cambridge, CB3 0HE, United Kingdom

ABSTRACT The bulk nanomorphology of organic bulk heterojunction devices, particularly of all-polymer devices, is difficult to characterize due to limited electron density contrast between constituent materials. Resonant soft X-ray scattering can overcome this problem and is used to show that the morphologies in chloroform cast and subsequently annealed polyfluorene copolymers poly(9,9′-dioctylfluorene-*co*-bis(*N*,*N*′-(4,butylphenyl))bis(*N*,*N*′-phenyl-1,4-phenylene)diamine) (PFB) and poly(9,9′-dioctylfluorene-*co*-benzothiadiazole) (F8BT) blends exhibit a hierarchy of length scales with impure domains in as-cast films. With annealing, these domains first become purer at the smallest length scale and only then evolve in size with annealing. Even optimized cells using present fabrication methods are found to have a dominant domain size much larger than the exciton diffusion length. The observed morphology is far from ideal for efficient solar cell operation and very different from those achieved in high-efficiency fullerene-based devices. This strongly implies that lack of morphological control contributes to the relatively poor performance of the all-polymer PFB:F8BT devices and may be problematic for all-polymer devices in general. Novel processing strategies will have to be employed to harness the full potential these high open circuit voltage devices offer.

KEYWORDS Polymer blends, X-ray scattering, organic solar cells, morphology

Solution-processed organic solar cells have attracted a great deal of attention recently due to their potential as a low-cost photovoltaic technology.[1] Currently, the most studied solar cell designs are based on bulk heterojunction (BHJ) structures, in which organic electron donor and electron acceptor materials form an interpenetrating network with the goal of optimizing photon absorption, exciton separation, and charge transport.[2,3] Commonly discussed is an "ideal morphology", whereby interconnected, pure phases with domain size of order of the exciton diffusion length (~10 nm) optimize exciton dissociation and a film thickness of 100−200 nm optimizes photon absorption. Indeed, many reports can be found claiming control of the nanomorphology[4,5] despite the fact that our ability to characterize film nanomorphology is limited. In order to establish full control over nanomorphology, one needs to control not only the characteristic, i.e., average domain size, but also the domain size distribution, domain purity, and domain interface widths. Given the heuristic fashion in which phase separation in polymer blends is manipulated, namely, by varying blend ratio,[6,7] molecular weight,[8] solvent choice,[9] solution concentration,[10] film drying time,[11] cosolvent/processing aids,[12,13] and annealing,[4,14] such full control of nanomorphology should not necessarily be expected. The goal of controlling the nanomorphology of organic photovoltaic blends depends therefore on developing not only new processing approaches but also upon new approaches to characterizing the created nanomorphologies. A recent review by Giridharagopal et al. highlights the challenges in characterizing morphology of organic photovoltaics at multiple length scales.[15] Characterization of the three-dimensional structure of organic blends with sub-10-nm resolution poses a key technical challenge. Most high-resolution techniques such as hard X-ray scattering[16] and transmission electron microscopy (TEM)[17] rely on differences in electron density for obtaining contrast in organic materials. This approach has been quite successful for the study of polymer/fullerene blends, for which a sufficient electron density difference exists. In particular recent electron tomography measurements have revealed three-dimensional structure in unprecedented detail.[18] However the chemical selectivity of these techniques is limited, for example, in the 3D tomography measurements only the crystalline (and not amor-

* To whom correspondence should be addressed: tel, +44 1223 337287 (C.R.M.) and (919) 515-1331 (H.A.); e-mail, crm51@cam.ac.uk (C.R.M.) and harald_ade@ncsu.edu (H.A.).

[||] Permanent address: Synchrotron SOLEIL, L'Orme des Merisiers, Saint-Aubin - BP 48 F-91192 Gif-sur-Yvette cedex, France.

[#] Permanent address: Paul Scherrer Institute, 5232 Villigen PSI, Switzerland.

[▽] Permanent address: Laboratoire de Chimie Physique, Université Pierre et Marie Curie (Paris VI), 11 rue Pierre et Marie Curie, 75005 Paris, France.

Received for review: 03/16/2010
Published on Web: 00/00/0000

DOI: 10.1021/nl1009266 | *Nano Lett.* **XXXX,** *xxx,* 000–000

phous) polymer regions could be distinguished from fullerene,[18] and information regarding domain purity cannot be accessed. Furthermore, there is little electron density contrast for polymer/polymer blends, limiting the use of TEM and small-angle X-ray scattering for these materials.

Historically, polymer/polymer blends have demonstrated lower efficiencies compared to their polymer/fullerene counterparts but are still of interest due to their higher open-circuit voltages and potential to create well-ordered nanostructures through the use of block copolymers.[19,20] Indeed, differences in morphology between these two materials systems may help explain their difference in performance, but with little direct morphological information on polymer/polymer blends a meaningful comparison is hard to make. Here, we demonstrate the use of resonant soft X-ray scattering (R-SoXS) in a transmission geometry to directly investigate the bulk nanostructure of BHJ films at high spatial resolution.[21,22] Due to the lower photon energy of soft X-rays that match the energy of core levels of the constituent atoms and specific spectral transitions, R-SoXS provides greatly enhanced scattering contrast and scattering intensity over conventional hard X-ray small angle scattering and also, in contrast to neutron scattering, does not require deuteration.[21,23] Furthermore, differences in the optical constants at soft X-ray energies of the constituent materials in the blend provides information regarding domain purity in addition to characterizing the distribution of domain sizes down to a few nanometers. This allows the investigation of polymer/fullerene and polymer/polymer systems and their direct comparison. Our experiments indicate that in contrast to the polymer/fullerene system, which exhibits a rather well-defined morphology with a small domain size distribution and domains ~20 nm in size, the polymer/polymer system contains a broad distribution of domain sizes with an average size far from the ideal nanomorphology of a single characteristic domain size of ~10 nm.

In order to characterize the nanomorphology in a model semiconducting polymer/polymer blend, we have investigated blends of the polyfluorene copolymers poly(9,9′-dioctylfluorene-*co*-bis(*N*,*N*′-(4,butylphenyl))bis(*N*,*N*′-phenyl-1,4-phenylene)diamine) (PFB) and poly(9,9′-dioctylfluorene-*co*-benzothiadiazole) (F8BT). Although having a rather poor photovoltaic efficiency, the device physics and photophysics of this system have been well-studied, thus making it a useful prototype system.[24−26] In particular, devices made with films prepared in an identical fashion as those investigated here have been studied previously, with the details of device performance and device physics published elsewhere.[27] A direct comparison to results presented here can thus be made. The chemical-specific contrast afforded by soft X-rays has been previously exploited to study the phase-separated structure of PFB/F8BT blends using scanning transmission X-ray microscopy (STXM).[28,29] While readily applicable to blends cast from *p*-xylene that exhibit relatively coarse morphologies,[28] the intrinsic resolution of ~35 nm for STXM[30] presents a limitation to characterize films processed from low-boiling-point solvents such as chloroform, which have much finer morphologies than those cast from *p*-xylene. When the nanomorphology of 150 nm thick PFB/F8BT films cast from chloroform were investigated, the smallest domain size detected with STXM was ~70−80 nm.[28] Whether this was indeed the intrinsic size of the domains or a spatial resolution limitation due to the film thickness could not be independently assessed. However, the existence of a finer nanomorphology or impure domains is inferred from photoluminescence quenching with as-cast films from chloroform showing an exciton dissociation efficiency of greater than 95%.[26] Furthermore, Westenhoff et al. have used exciton diffusion modeling in combination with femtosecond transient absorption spectroscopy to deduce the distribution of domain sizes in chloroform-cast blends of PFB and F8BT and also demonstrated sub-10-nm structure.[31] We note, however, that such exciton diffusion modeling requires assumptions regarding the nature of exciton diffusion and does not represent a direct measurement of nanostructure. Furthermore, only structures as large as the exciton diffusion length can be probed.

PFB/F8BT blends with a 1:1 weight ratio were cast from chloroform onto poly(3,4-ethylenedioxythiophene)polystyrene sulfonic acid coated glass slides to a thickness of ~150 nm. As-cast films or films annealed for 10 min on a hot plate were floated onto a 5 mm × 5 mm silicon frame with a 1 mm × 1 mm opening. PFB and F8BT were supplied by Cambridge Display Technology (CDT) Ltd. with molecular weights of M_p ~135 kg/mol and M_p ~150 kg/mol, respectively. In a similar manner, P3HT/PCBM blends were spin-cast with 1:1 weight ratio from chlorobenzene solution to a thickness of ~150 nm, annealed at 140 °C for 2 h, and transferred to a 5 mm × 5 mm silicon frame supporting a 1 mm × 1 mm, 100 nm thick Si_3N_4 membrane. Regioregular (93%) P3HT and PCBM were supplied by American Dye Source Inc. The molecular weight of P3HT was 60 kg/mol. STXM measurements were performed at beamline 5.3.2 of the Advanced Light Source (ALS), Berkeley, CA.[30] The silicon frame-supported films were mounted in the sample chamber which was evacuated to 0.3 mbar and subsequently refilled with $^1/_3$ atm of helium. The intensity of the focused X-ray beam transmitted through the film was recorded using a scintillator and photomultiplier tube and measured as a function of energy and position. Images were acquired at 285.1 eV, the energy that provides the maximum compositional contrast.[32] R-SoXS measurements[21,23] of PFB/F8BT were performed at beamline 6.3.2 of the ALS.[33] A 600 L/mm grating was used in combination with an exit slit width of 80 μm to monochromatize the beam. A channeltron was used as the detector. The photon energy was calibrated by measuring absorption spectra at the beamline and by comparison with near edge absorption features of known spectra.[34] Scattering was performed at 284.8 and 285.2 eV for the PFB/F8BT and P3HT/PCBM systems, respectively. These photon energies provide maximum scattering intensity for the particular samples. Due to radiation sensitivity, the P3HT/PCBM system was

DOI: 10.1021/nl1009266 | *Nano Lett.* **XXXX,** *xxx,* 000−000

NANO LETTERS

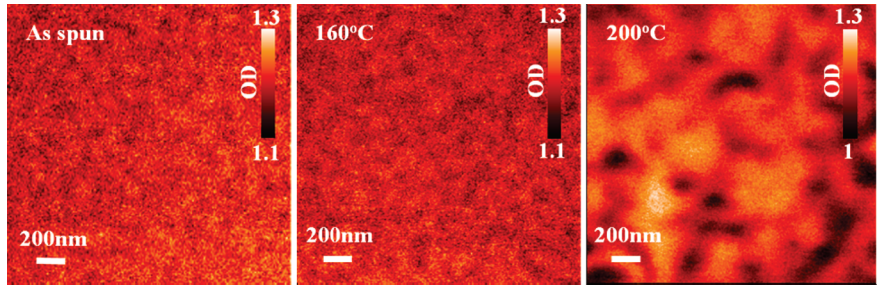

FIGURE 1. STXM images (2 μm × 2 μm) displayed in optical density (OD) of polymer blends annealed for 10 min at temperatures as indicated. Data acquired at 285.1 eV. Images are individually scaled for contrast as indicated.

investigated at the soft X-ray coherent scattering beamline 5-2 of the SSRL where a CCD detector was used to acquire data with much lower dose. However, the use of a beamstop that was not yet optimized in size blocked the scattering at small values of scattering vector **q**.

F1 Figure 1 presents STXM images of PFB/F8BT blends with phase separation noticeably increasing with annealing at 200 °C. Features exhibiting an average size of ~80 nm are observed for the as-spun films. The contrast for these features however is very low, indicating mixed composition and/or a three-dimensional morphology of which only the projection is measured. The mean feature size increases to ~85 nm for films annealed at 160 °C and increases further to ~100 and ~250 nm for films annealed at 180 °C (not shown) and 200 °C, respectively. A summary is provided in Table 1. A significant intermixing in these domains with a hierarchy of phase separation existing on a length scale of less than 100 nm in the unannealed and mildly annealed sample was previously hypothesized from prior photoluminescence measurements and the use of Monte Carlo simulations of exciton diffusion that used a single dominant length scale.[29] However, this nanomorphology cannot be readily characterized in the bulk with existing real-space, i.e., microscopy, methods.

Significantly more nuanced and higher spatial resolution information than available from STXM can be achieved with R-SoXS experiments. This is a scattering, i.e. reciprocal space method, that has only recently been applied to investigate polymer systems.[21,23,35] A detailed overview of X-ray scattering as a technique is available in ref 35. The advantage of R-SoXS stems from the ability to achieve much higher scattering intensities in relation to hard X-rays small angle scattering and thus is able to characterize the bulk of very thin films in transmission. The energy dependence of the measured intensity $I(E)$ in a small angle or long wavelength limit X-ray scattering experiment is given as

$$I(E) \propto F^2(E) \propto E^4 |\Delta\delta(E) + i\Delta\beta(E)|^2 \qquad (1)$$

Here, E is the photon energy and F is the scattering factor. In the soft X-ray region, one is operating in the long

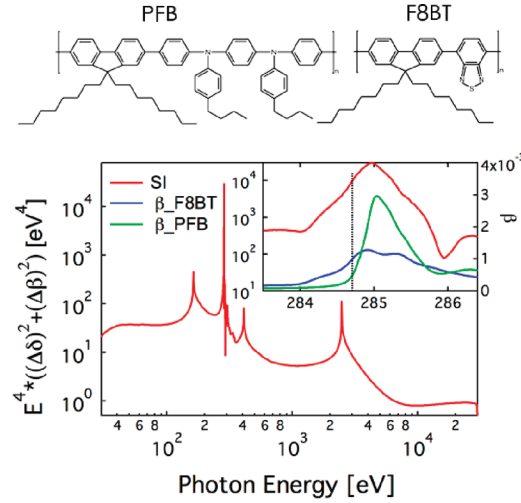

FIGURE 2. Relative scattering intensity (SI) for a PFB/F8BT thin film with pure domains and with a fixed thickness of a fraction of an absorption length (<30 nm). Inset shows the theoretical scattering intensity for PFB/F8BT and the absorption coefficient β of PFB and F8BT near the carbon absorption edge. The chemical structures of PFB and F8BT are provided above the graph.

wavelength limit and the q (scattering vector) dependence of F can be neglected. F can be described in terms of $\Delta\delta$ and $\Delta\beta$, the differences in the dispersive and absorptive components, respectively, of the complex index of refraction between two phases. Given that hard X-rays have energy much larger than the energy of the deepest core levels of constituent atoms in most polymers, eq 1 implies that the scattering intensity for hard X-rays is mostly determined by the total electron density contrast between polymeric materials. Near resonance, however, the intensity is modulated strongly by the rapid changes in either dispersion or absorption and can even be dominated by absorption, i.e., $\Delta\beta^2$. Furthermore scattering is vastly enhanced near an absorption edge for soft X-rays as the $\Delta\delta^2 + \Delta\beta^2$ factor can overcome the E^4 factor. In order to exemplify this strength in the context of materials important to organic device research in general and the specific study presented here, we show in Figure 2 the F2 relative scattering intensity of a PFB:F8BT thin film with pure domains and with a fixed thickness that is a fraction of the photon absorption length (<30 nm). Experiments utilizing the maximum scattering peak near the carbon

DOI: 10.1021/nl1009266 | *Nano Lett.* **XXXX,** *xxx,* 000–000

NANO LETTERS

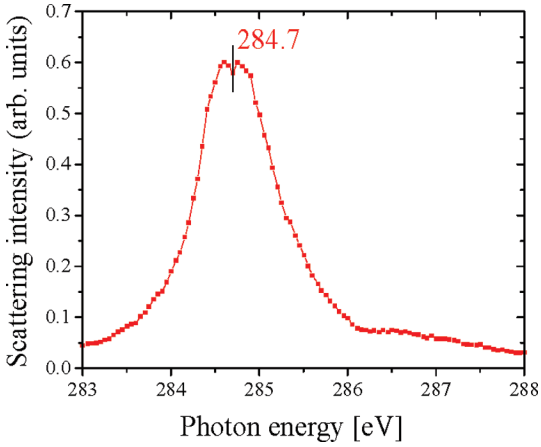

FIGURE 3. Energy scan at fixed detector angle of $2\theta = 1°$ for sample annealed at 140 °C.

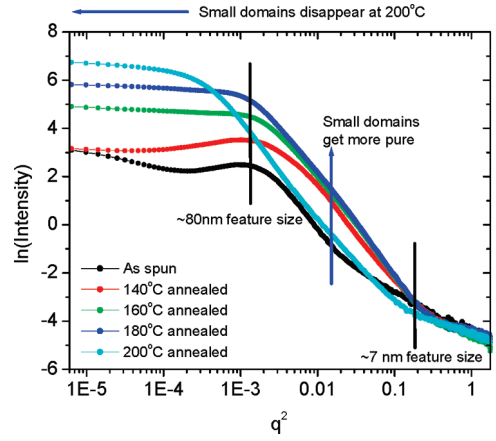

FIGURE 4. Scattering profiles of PFB/F8BT blends acquired at 284.7 eV and plotted as ln(I) vs q^2.

absorption edge yield orders of magnitude higher scattering intensities than at other energies. This allows acquisition of useful data on very thin films even with a relatively low flux bending magnet beamline such as the ALS BL 6.3.2 and an angle-inefficient 1D detector. Additionally, the relative purity of the domains in the films can be ascertained as the absolute and relative scattering intensity at constant energies scales with $\Delta\delta^2 + \Delta\beta^2$, which in turn reflects the purity of the domains. For examples, domains with PFB:F8BT composition of 75/25 and 25/75 for the two phases, respectively, will only yield $^1/_4$th the scattering intensity of samples with pure domains.

The 150 nm thick films of interest here exhibit ~50% absorption at photon energies corresponding to the strong absorption resonance of PFB at ~285 eV. The best condition for scattering was thus ascertained experimentally by performing an energy scan at fixed detector angle ($2\theta = 1°$) reproduced in Figure 3. These data indicate that the best energy for detector scans is ~284.7 eV, just off the peak expected for yet thinner films. This energy is marked with a dotted line in the inset of Figure 2. It is below the strong absorption peak of PFB and phase differences resulting from $\Delta\delta^2$ make an important if not dominant contribution to the scattering contrast. This situation is analogous to the case of hard X-ray scattering on low Z materials, which predominately relies on differences in $\Delta\delta^2$. Yet, due to the resonant enhancement, the phase differences between the two materials are much larger just below the carbon absorption edge than at high energy, which amplifies the scattering intensity.

The background subtracted scattering profiles of 150 nm thin films of PFB/F8BT polymer blends, which were annealed at different temperatures, are shown in Figure 4 as a function of the scattering vector $q = (4\pi/\lambda)\sin(\theta)$, where 2θ is the angle between the detector and the transmitted beam and λ is the photon wavelength. The intensities were normalized for small thickness variations using absorption measurements in transmission. The profiles are plotted as ln(I) vs q^2 for a better visualization of the relative intensities at low q. Qualitatively, the scattering intensities show significant differences which can be interpreted by considering that small features yield scattering intensity at high q, large features contribute at low q, and that "monodisperse" domains yield oscillations in the scattering intensity. The curve of the as-cast film shows the lowest overall scattering intensity, a well-defined peak at $q = 0.04$ nm^{-1}, and an easy to make out shoulder at $q = 0.4$ nm^{-1}. The lack of strong modulations and low scattering intensity indicates that the sample has domains at multiple length scales that are not very pure. The best defined domains have a size of ~70−80 nm and the small scattering feature corresponds to domains ~7 nm in size, After annealing at 140 °C, the scattering intensity increases significantly only for $q > 0.01$ nm^{-1}, with a particular pronounced increase for $q \sim 0.1-0.2$ nm^{-1}. No single dominant domain size with a characteristic scattering peak emerges due to annealing. Domains smaller than 60 nm become purer and possibly more numerous. Annealing at 160 °C yields relatively little further increases in scattering intensity for $q > 0.07$ nm^{-1}, but significant increases for $q < 0.05$ nm^{-1}. The smallest domain must have nearly reached their equilibrium composition and only the larger domains can further phase separate toward the equilibrium composition. This trend continues for annealing at 180 °C. Annealing at 200 °C then yields a new regime, in which the smallest domains are completely lost due to coarsening (increased intensity at low q and relative loss of $I(q)$ at large q) and the average domain size increases significantly as indicated by the q value at which the intensity starts to decrease substantially. The shape of the scattering intensity, i.e., absence of oscillations or clear peaks, indicates a large dispersion of domain sizes. The shape and the changes in the shape of the scattering intensity show clearly that the structure factor of the morphological evolution is not governed by a scale-invariant or a scaling relationship as one observes during the initial phase separation and coarsening of a spinodal decomposition process.

These qualitative inferences from the scattering intensity can also be observed readily and with additional quantitative

DOI: 10.1021/nl1009266 | *Nano Lett.* **XXXX,** *xxx,* 000–000

NANO LETTERS

TABLE 1. Dominant Domain Sizes Derived from STXM and R-SoXS and Maximum Value of $P(r)$

sample		as spun	140 °C	160 °C	180 °C	200 °C
domain size	R-SoXS	~77 nm	~71 nm	~89 nm	~110 nm	~260 nm
	STXM	~80 nm	~80 nm	~85 nm	~100 nm	~250 nm
$P(r)_{max}$	R-SoXS	0.028	0.082	0.21	0.43	0.46

nuances by examining the pair distance distribution function,[36] $P(r)$, as calculated from the scattering intensity by

$$P(r) = \frac{r}{2\pi^2}\int_0^\infty I(q)q\sin(qr)\,dq \qquad (2)$$

$P(r)$ is related to the frequency of certain distances r within the sample, i.e., the number of like molecules in a thin shell a distance r from any given point in the sample. It thus provides assemble average information about the distances between the phases in the sample and the shape of the domains. The first zero crossing of $P(r)$ is an indication of the mean domain size. Since $I(q)$ scales with the contrast factor $(\Delta\delta^2 + \Delta\beta^2)$, so does $P(r)$ and the magnitude of the first peak for a given $P(r)$ is a measure of the purity of the phases.[36] Considering $P(r)$ for the six temperatures investigated (see Figure 3), and the scaling of $P(r)$ with $(\Delta\delta^2 + \Delta\beta^2)$, annealing at 140 °C clearly yields slightly smaller but significantly purer domains than the as-cast film. Annealing at 160 and 180 °C results primarily in purer domains yet with roughly a doubling of the $P(r)$ peak and a much smaller increase in domain size as measured by the first zero crossing of $P(r)$. The peak values of $P(r)$ and the domain sizes as measured by the zero crossing are summarized in Table 1 and shown graphically in Figure 5. Finally, annealing at 200 °C results primarily in coarsening, which is characterized by an increase in domain size. Overall, domain size increases from ~77 nm for the as-spun films to ~260 nm for the film annealed at 200 °C, with a small, temporary decrease to ~71 nm observed for the film annealed at 140 °C, the lowest temperature utilized. These domain sizes measured with R-SoXS correlate to the STXM measurements, but, in addition, the $P(r)$ functions clearly show that there is no dominant morphology at a length scale smaller than that detected with STXM. Hence, the average domains in all blends are substantially larger than the exciton diffusion length, yet the low domain contrast in STXM and with R-SoXR in the as-cast film directly implies molecular level mixing in these films.

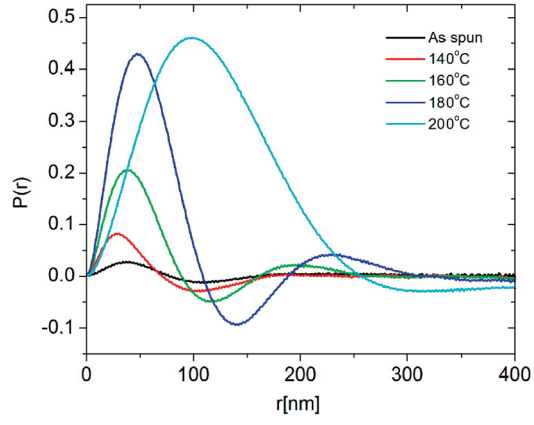

FIGURE 5. Pair distance distribution function P(r) for scattering profiles from PFB:F8BT samples as shown in figure 2.

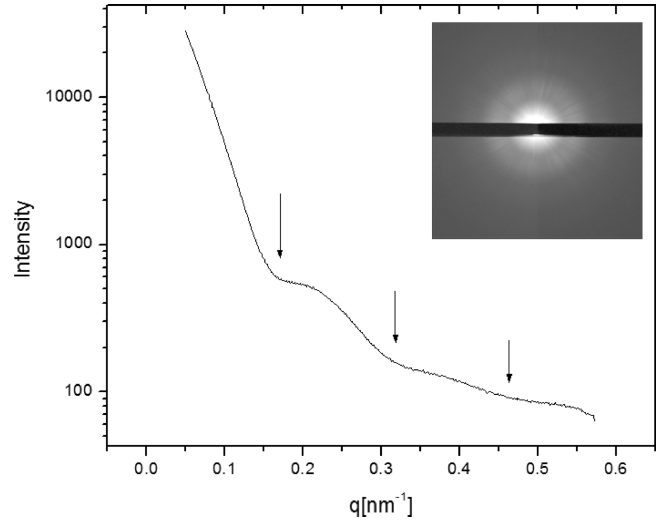

FIGURE 6. Radially averaged R-SoXS intensity at 285.2 eV for 150 nm thick P3HT/PCBM film annealed at 140 °C for 2 h and acquired at SSRL BL 5-2 with a CCD detector. Inset image shows the background subtracted CCD scattering data in log scale.

To contrast the R-SoXS results for the PFB:F8BT films, R-SoXS data for P3HT/PCBM thin films are shown in Figure 6. The inset shows the raw data from the CCD with a relatively large stop to block the central high intensity beam. The radially averaged scattering density displayed in Figure 6 shows clearly delineated oscillating peaks corresponding to domains ~20 nm in size ($\pi/\Delta q$), consistent with the domain size measured by grazing incidence hard X-ray scattering.[16] The need to use a central stop for the CCD prevented the acquisition of information from the low scattering vector (q) range which is required to calculate a meaningful pair distribution function. Therefore, the data in Figure 6 need to be interpreted qualitatively. The oscillating nature of the P3HT/PCBM scattering intensity is in stark contrast to the data of the PFB/F8BT system. The observed oscillations furthermore clearly indicate that P3HT/PCBM blends relatively readily phase separate into a structure with a dominant domain size and relatively narrow size distribution. This is consistent with previous TEM observations,[17] and the mean domain size of ~20 nm is furthermore significantly smaller than the size observed for PFB/F8BT and thus better matched to the exciton diffusion length. We expect that less aggressively annealed P3HT/PCBM samples would have even smaller domains.[17]

Our observation of relatively poor control over nanomorphology in PFB/F8BT blends using standard processing

DOI: 10.1021/nl1009266 | *Nano Lett.* **XXXX,** *xxx,* 000–000

routes has implications for the ultimate efficiency that can be achieved by all-polymer blends. Clearly to optimize device performance, a narrow domain size distribution centered about the exciton diffusion length (or slightly larger) is required in order to maximize the processes of exciton dissociation and charge separation. Having a broad distribution of domain sizes even in the 140 °C annealed film that optimizes device performance as previously shown implies that some excitons will be wasted as they will not be able to reach heterointerfaces while some interfacial charge pairs will not be able to separate due to a constrictive local morphology. While unfavorable interfacial electronic properties of PFB/F8BT blends (namely, exciplex formation and strong geminate recombination)[37] most likely accounts for the lower efficiency of the PFB/F8BT system in comparison to more efficient all-polymer systems. A recent report has shown that a novel cross-linking based approach to create nanostructured PFB/F8BT heterostructure devices with pure phases was able to achieve higher efficiencies than have been attained with devices utilizing solution-processed blends.[38] Furthermore, it is also likely that this poor control of morphology exists even for other all-polymer systems, despite annealing procedures to optimizing their efficiency.[39−41] Therefore, a key challenge for realizing high efficiency all-polymer cells and enabling exploitation of their high open-circuit voltage is achieving better morphological control. Comparison of morphologies of annealed and cosolvent processed PFB/F8BT has suggested similar morphologies are produced by these processing routes,[42] so new processes that provide more exquisite morphological control will need to be developed. A number of approaches are currently being developed including nanoimprint lithography[43] and diblock copolymers[44] (as well as the cross-linking approach mentioned above[38]). These early results encourage further effort in this direction.

In summary, we have demonstrated the utility of resonant soft X-ray scattering to probe the bulk structure and domain composition of the active layer of organic bulk heterojunction solar cells with sub-10-nm resolution. The high scattering intensity and superior chemical contrast achieved with soft X-rays allows for scattering experiments to be conducted on thin films in a transmission geometry and provides information regarding the domain size distribution of all-polymer blends for which little contrast exists using other techniques. Furthermore, R-SoXS investigations of the all-polymer photovoltaic model system PFB/F8BT demonstrated that the morphology and domain composition in these systems cannot be controlled very well by casting and annealing. For all conditions investigated, including annealing at 140 °C which had previously yielded the highest power conversion efficiency,[25] the dominant domain size directly measured with R-SoXS is substantially larger than the exciton diffusion length. Furthermore, these domains are initially rather impure in composition (or composed of domains smaller than the ∼1−2 nm scale probed here) indicating a nearly homogeneous starting condition that explains the very high photoluminescence quenching yet low external quantum efficiency for these samples. None of the morphologies created for PFB/F8BT and characterized by R-SoXS is close to the ideal morphology of small and pure domains. This is in contrast to the high external quantum efficiency fullerene-based system, which exhibits a well-defined morphology in P3HT/PCBM samples at length scales smaller than those observed for the PFB/F8BT blends and closer in size to the exciton diffusion length. This helps to explain the relatively poor efficiency of all-polymer systems and clearly implies that insufficient morphological control is a major negative factor on such systems. Novel processing routes and device fabrication processes that provide superior morphological control will have to be developed to harness the high V_{OC} potential exhibited by all-polymer devices.

Acknowledgment. Work by NCSU was supported by the US Department of Energy, Office of Science, Basic Energy Science, Division of Materials Science and Engineering for support under Contract DE-FG02-98ER45737. ALS is supported by the US Department of Energy, Office of Basic Energy Science. Portions of this research were carried out at SSRL (BL 5-2), a national user facility operated by Stanford University on behalf of the US Department of Energy, Office of Basic Energy Science. C.R.M. acknowledges the EPSRC for provision of an Advanced Research Fellowship. The authors are thankful to E. Gullikson (CXRO, LBNL), A. L. D. Kilcoyne (ALS), and W. Schlotter (while at Stanford University) for support during these experiments. The authors also thank Cambridge Display Technology Ltd. for supply of PFB and F8BT.

REFERENCES AND NOTES

(1) Gunes, S.; Neugebauer, H.; Sariciftci, N. S. *Chem. Rev.* **2007**, *107* (4), 1324–1338.
(2) Halls, J. J. M.; Walsh, C. A.; Greenham, N. C.; Marseglia, E. A.; Friend, R. H.; Moratti, S. C.; Holmes, A. B. *Nature* **1995**, *376* (6540), 498–500.
(3) Yu, G.; Gao, J.; Hummelen, J. C.; Wudl, F.; Heeger, A. J. *Science* **1995**, *270* (5243), 1789–1791.
(4) Ma, W.; Yang, C.; Gong, X.; Lee, K.; Heeger, A. J. *Adv. Funct. Mater.* **2005**, *15*, 1617–1622.
(5) Radbeh, R.; Parbaile, E.; Bouclé, J.; Di Bin, C.; Moliton, A.; Coudert, V.; Rossignol, F.; Ratier, B. *Nanotechnology* **2010**, *21*, No. 035201.
(6) Snaith, H. J.; Arias, A. C.; Morteani, A. C.; Silva, C.; Friend, R. H. *Nano Lett.* **2002**, *2* (12), 1353–1357.
(7) van Duren, J. K. L.; Yang, X.; Loos, J.; Bullie-Lieuwma, C. W. T.; Sieval, A. B.; Hummelen, J. C.; Janssen, R. A. J. *Adv. Funct. Mater.* **2004**, *14* (5), 425–434.
(8) Snaith, H. J.; Friend, R. H. *Thin Solid Films* **2004**, *451−52*, 567–571.
(9) Shaheen, S. E.; Brabec, C. J.; Sariciftci, N. S.; Padinger, F.; Fromherz, T.; Hummelen, J. C. *Appl. Phys. Lett.* **2001**, *78* (6), 841–843.
(10) Hoppe, H.; Niggemann, M.; Winder, C.; Kraut, J.; Hiesgen, R.; Hinsch, A.; Meissner, D.; Sariciftci, N. S. *Adv. Funct. Mater.* **2004**, *14* (10), 1005–1011.
(11) Li, G.; Shrotriya, V.; Huang, J. S.; Yao, Y.; Moriarty, T.; Emery, K.; Yang, Y. *Nat. Mater.* **2005**, *4* (11), 864–868.
(12) Peet, J.; Kim, J. Y.; Coates, N. E.; Ma, W. L.; Moses, D.; Heeger, A. J.; Bazan, G. C. *Nat. Mater.* **2007**, *6* (7), 497–500.
(13) Campbell, A. R.; Hodgkiss, J. M.; Westenhoff, S.; Howard, I. A.; Marsh, R. A.; McNeill, C. R.; Friend, R. H.; Greenham, N. C. *Nano Lett.* **2008**, *8* (11), 3942–3947.

DOI: 10.1021/nl1009266 | *Nano Lett.* **XXXX,** *xxx,* 000–000

NANO LETTERS

(14) Padinger, F.; Rittberger, R. S.; Sariciftci, N. S. *Adv. Funct. Mater.* **2003**, *13* (1), 85–88.
(15) Giridharagopal, R.; Ginger, D. S. *J. Phys. Chem. Lett.* **2010**, *1* (7), 1160–1169.
(16) Chiu, M. Y.; Jeng, U. S.; Su, C. H.; Liang, K. S.; Wei, K. H. *Adv. Mater.* **2008**, *20* (13), 2573–2578.
(17) Yang, X.; Loos, J.; Veenstra, S. C.; Verhees, W. J. H.; Wienk, M. M.; Kroon, J. M.; Michels, M. A. J.; Janssen, R. A. J. *Nano Lett.* **2005**, *5* (4), 579–583.
(18) van Bavel, S. S.; Sourty, S.; de With, G.; Loos, J. *Nano Lett.* **2009**, *9* (2), 507–513.
(19) McNeill, C. R.; Greenham, N. C. *Adv. Mater.* **2009**, *21* (38−39), 3840–3850.
(20) Veenstra, S. C.; Loos, J.; Kroon, J. M. *Prog. Photovoltaics* **2007**, *15*, 727–740.
(21) Araki, T.; Ade, H.; Stubbs, J. M.; Sundberg, D. C.; Mitchell, G. J. K.; Kilcoyne, A. L. D. *Appl. Phys. Lett.* **2006**, *89* (12), 124106.
(22) Ade, H.; Hitchcock, A. P. *Polymer* **2008**, *49* (3), 643–675.
(23) Mitchell, G. E.; Landes, B. G.; Lyons, J.; Kern, B. J.; Devon, M. J.; Koprinarov, I.; Gullikson, E. M.; Kortright, J. B. *Appl. Phys. Lett.* **2006**, *89* (4), No. 044101.
(24) Halls, J. J. M.; Arias, A. C.; MacKenzie, J. D.; Wu, W. S.; Inbasekaran, M.; Woo, E. P.; Friend, R. H. *Adv. Mater.* **2000**, *12* (7), 498.
(25) Ramsdale, C. M.; Barker, J. A.; Arias, A. C.; MacKenzie, J. D.; Friend, R. H.; Greenham, N. C. *J. Appl. Phys.* **2002**, *92* (8), 4266–4270.
(26) McNeill, C. R.; Westenhoff, S.; Groves, C.; Friend, R. H.; Greenham, N. C. *J. Phys. Chem. C* **2007**, *111* (51), 19153–19160.
(27) McNeill, C. R.; Westenhoff, S.; Groves, C.; Friend, R. H.; Greenham, N. C. *J. Phys. Chem. C* **2007**, *111* (51), 19153–19160.
(28) McNeill, C. R.; Watts, B.; Swaraj, S.; Ade, H.; Thomsen, L.; Belcher, W. J.; Dastoor, P. C. *Nanotechnology* **2008**, *19* (42), 424015.
(29) McNeill, C. R.; Watts, B.; Thomsen, L.; Ade, H.; Greenham, N. C.; Dastoor, P. C. *Macromolecules* **2007**, *40* (9), 3263–3270.
(30) Kilcoyne, A. L. D.; Tyliszczak, T.; Steele, W. F.; S., F.; Hitchcock, P.; Franck, K.; Anderson, E. H.; Harteneck, B. D.; Rightor, E. G.; Mitchell, G. E.; Hitchcock, A. P.; Yang, L.; Warwick, T.; Ade, H. *J. Synchrotron Radiat.* **2003**, *10*, 125–136.
(31) Westenhoff, S.; Howard, I. A.; Friend, R. H. *Phys. Rev. Lett.* **2008**, *101*, No. 016102.
(32) McNeill, C. R.; Watts, B.; Thomsen, L.; Belcher, W.; Swaraj, S.; Ade, H.; Dastoor, P. C. *Nanotechnology* **2008**, *19* (42), 424015.
(33) Underwood, J. H.; Gullikson, E. M. *J. Electron Spectrosc. Relat. Phenom.* **1998**, *92* (1−3), 265–272.
(34) Dhez, O.; Ade, H.; Urquhart, S. *J. Electron Spectrosc. Relat. Phenom.* **2003**, *128* (1), 85–96.
(35) Virgili, J. M.; Tao, Y. F.; Kortright, J. B.; Balsara, N. P.; Segalman, R. A. *Macromolecules* **2007**, *40* (6), 2092–2099.
(36) Glatter, O.; Kratky, O. *Small Angle X-Ray Scattering*; Academic Press: New York, 1982.
(37) Gonzalez-Rabade, A.; Morteani, A. C.; Friend, R. H. *Adv. Mater.* **2009**, *21*, 3924–3927.
(38) Png, R. Q.; Chia, P. J.; Tang, J. C.; Liu, B.; Sivaramakrishnan, S.; Zhou, M.; Khong, S. H.; Chan, H. S. O.; Burroughes, J. H.; Chua, L. L.; Friend, R. H.; Ho, P. K. H. *Nat. Mater.* , *9* (2), 152–158.
(39) Kietzke, T.; Hörhold, H.-H.; Neher, D. *Chem. Mater.* **2005**, *17*, 6532–6537.
(40) Koetse, M. M.; Sweelssen, J.; Hoekerd, K. T.; Schoo, H. F. M.; Veenstra, S. C.; Kroon, J. M.; Yang, X.; Loos, J. *Appl. Phys. Lett.* **2006**, *88*, No. 083504.
(41) McNeill, C. R.; Halls, J. J. M.; Wilson, R.; Whiting, G. L.; Berkebile, S.; Ramsey, M. G.; Friend, R. H.; Greenham, N. C. *Adv. Funct. Mater.* **2008**, *18* (16), 2309–2321.
(42) Campbell, A. J. Charge-Pair Generation and Separation in Solution-Processable Solar Cells. PhD Thesis, University of Cambridge, 2009.
(43) He, X.; Gao, F.; Tu, G.; Hasko, D.; Hüttner, S.; Steiner, U.; Greenham, N. C.; Friend, R. H.; Huck, W. T. S. *Nano Lett.* **2010**, *10* (4), 1302–1307.
(44) Sommer, M.; Huttner, S.; Steiner, U.; Thelakkat, M. *Appl. Phys. Lett.* **2009**, *95* (18), 183308.

DOI: 10.1021/nl1009266 | *Nano Lett.* **XXXX,** *xxx,* 000–000